

CIGALEMC: GALAXY PARAMETER ESTIMATION USING A MARKOV CHAIN MONTE CARLO APPROACH WITH CIGALE

PAOLO SERRA¹, ALEXANDRE AMBLARD¹, PASQUALE TEMI¹, DENIS BURGARELLA², ELODIE GIOVANNOLI²,
 VERONIQUE BUAT², STEFAN NOLL³, STEPHEN IM¹

Draft version February 24, 2024

ABSTRACT

We introduce a fast Markov Chain Monte Carlo (MCMC) exploration of the astrophysical parameter space using a modified version of the publicly available code CIGALE (Code Investigating GALaxy emission). The original CIGALE builds a grid of theoretical Spectral Energy Distribution (SED) models and fits to photometric fluxes from Ultraviolet (UV) to Infrared (IR) to put constraints on parameters related to both formation and evolution of galaxies. Such a grid-based method can lead to a long and challenging parameter extraction since the computation time increases exponentially with the number of parameters considered and results can be dependent on the density of sampling points, which must be chosen in advance for each parameter. Markov Chain Monte Carlo methods, on the other hand, scale approximately linearly with the number of parameters, allowing a faster and more accurate exploration of the parameter space by using a smaller number of efficiently chosen samples. We test our MCMC version of the code CIGALE (called CIGALEMC) with simulated data. After checking the ability of the code to retrieve the input parameters used to build the mock sample, we fit theoretical SEDs to real data from the well known and studied SINGS sample. We discuss constraints on the parameters and show the advantages of our MCMC sampling method in terms of accuracy of the results and optimization of CPU time.

Subject headings: galaxies: fundamental parameters - methods: data analysis

1. INTRODUCTION

The spectral energy distribution (SED) of galaxies depends on many physical processes related to the emission from different stellar populations, absorption and re-emission from dust and gas and possible presence of Active Galactic Nuclei (AGN). Each process has been studied by many authors; libraries of stellar population models (Fioç & Rocca-Volmerange (1997), Bruzual & Charlot (2003), Maraston (2005)), fitting curves for dust emission (Calzetti et al. (1994, 2000), Witt & Gordon (2000)), studies of emission of dust grains (Chary & Elbaz (2001), Dale & Helou (2002), Lagache et al. (2003, 2004), and Siebenmorgen & Krügel (2007), Silva et al. (1998), Dopita et al. (2005), da Cunha et al. (2008)) are the basis of sophisticated fitting codes which derive physical parameters such as stellar mass, star formation rate, dust luminosity and so on.

Many parameters are usually necessary to describe these processes and model theoretical SEDs of galaxies. A grid of theoretical SED models is usually built and fitted to the data and statistical properties are derived for the parameters of interest. A big drawback of any grid-based method is that, for any fitting process, the time to build models grows linearly with the number of models and then about exponentially with the number of parameters involved: such approaches are difficult to implement for complex models involving a sufficiently large number of parameters or when a fine sampling of the pa-

rameter space is necessary in order to retrieve statistically robust results. In the past few years, Markov Chains Monte Carlo (MCMC) techniques have started being widely used in physics. In cosmology, parameter estimation from cosmic microwave background data with MCMC methods has been introduced in Christensen et al. (2001) and has been implemented in the publicly available code `cosmomc` (Cosmological Monte Carlo, Lewis & Bridle (2002))⁴; in astrophysics, an MCMC approach to the stellar population synthesis modeling has been introduced in Conroy et al. (2009).

Here we use `cosmomc` as a generic sampler and we interface it to the publicly available code CIGALE⁵ (Code Investigation GALaxy Emission, Noll et al. (2009)) in order to allow a fast and accurate evaluation of the multidimensional parameter space probed by this code⁶. The main advantage of this method is that the computing time to fit the data scales approximately linearly with the number of parameters involved, allowing the user to consider complex models with many parameters for only small additional computational time. MCMC techniques allow to probe also the shape of the probability distribution, giving far more information than just best fit and marginalized values for the parameters.

The paper is organized as follows; in the next section we briefly describe CIGALE, introducing the main parameters used in the subsequent sections. We then explain the MCMC technique implemented in the modified version of CIGALE, which we call CIGALEMC. We test our code

¹ Astrophysics Branch, NASA/Ames Research Center, MS 245-6, Moffett Field, CA 94035.

² Observatoire Astronomique de Marseille-Provence, 38 rue Frederic Joliot-Curie, 13388 Marseille Cedex 13, France.

³ Institut für Astro- und Teilchenphysik, Universität Innsbruck, Technikerstr.25/8, 6020 Innsbruck, Austria

⁴ <http://cosmologist.info/cosmomc/>

⁵ <http://www.oamp.fr/cigale/>

⁶ During the completion of this work we noticed that Acquaviva et al. (2011) have performed a similar work in the context of the code GALAXEV developed by Bruzual & Charlot (2003).

using a mock sample of 62 galaxies already used in Giovannoli *et al.* (2011) and we apply it to a real galaxy sample with data from the Spitzer Infrared Nearby Galaxy Survey (SINGS, see Kennicutt *et al.* (2003)). We always consider a flat cosmological model with $\Omega_m = 0.3$, $\Omega_\Lambda = 0.7$ and $H_0 = 70 \text{ km s}^{-1} \text{ Mpc}^{-1}$. Finally we give our results and conclusions.

2. THE CODE CIGALE

CIGALE calculates a grid of theoretical SEDs and fits to observational input data constituted by photometric filter fluxes ranging from UV to IR. For a detailed description of the code and its application to real data, we refer the interested reader to these papers (Burgarella *et al.* (2005), Noll *et al.* (2009), Giovannoli *et al.* (2011), Buat *et al.* (2011)). In the following, we briefly summarize its main characteristics and the basic parameters used in the next sections. Our notation follows the one introduced in Giovannoli *et al.* (2011).

2.1. Stellar populations and star formation rate

CIGALE combines both old and young stellar populations using single stellar populations of Maraston *et al.* (2005) or PEGASE (Fioc & Rocca-Volmerange (1997)). In this paper we will only use Maraston models; we assume star formation histories (SFH) with either exponentially decreasing star formation rate (SFR) in function of time t (“ τ models”), as:

$$\text{SFR}_{\text{old}}(t) = \text{SFR}_{0,\text{old}} \cdot e^{-\frac{(t-t_1)}{\tau_1}} \quad (1)$$

$$\text{SFR}_{\text{young}}(t) = \text{SFR}_{0,\text{young}} \cdot e^{-\frac{(t-t_2)}{\tau_2}}$$

or “box models” characterized by constant SFR over a limited period of time; in this case the instantaneous SFR at look-back time $t' = 0$ is given by the galaxy mass divided by the age t of the population, i.e. M_{gal}/t . Labels 1 and 2 refers to the old and young stellar populations while $\tau_{1,2}$ and $t_{1,2}$ (both in units of Gyr) are their e-folding time and age respectively. The two stellar populations are linked and weighted through their mass fraction; the parameter f_{ySP} represents the fraction of the young stellar mass over the total mass, so that the total instantaneous SFR (output parameter of CIGALE) is expressed as:

$$\text{SFR} = (1 - f_{\text{ySP}})\text{SFR}_{\text{old}}(t) + f_{\text{ySP}}\text{SFR}_{\text{young}}(t). \quad (2)$$

2.2. Absorption and emission by dust and gas

In CIGALE, the absorption of star light by dust is described by a Calzetti attenuation curve (Calzetti *et al.* (1994, 2000)); possible modifications of the curve include both the addition of a UV bump at about 2175Å (Fitzpatrick & Massa (1990; 2007); Noll *et al.* (2009)) and the change of the slope through the multiplication by a power law $(\lambda/\lambda_V)^\delta$, where $\lambda_V = 5500\text{Å}$ is the reference wavelength for the V filter; both the amplitude of the bump and the slope δ are free parameters of the code. The attenuation correction is applied to both stellar populations individually using the visual attenuation parameter of the young stellar populations (A_{ySP} , in units of magnitudes) and a reduction factor of the attenuation for the old model (f_V) as free parameters⁷.

The code also calculates 3 additional parameters, derived from the final model SEDs; A_{FUV} and A_V are defined as the effective attenuation factors in magnitudes at $1500 \pm 100\text{Å}$ and $5500 \pm 100\text{Å}$ while the age t_{D4000} is derived from the D4000 break (see Balogh *et al.* (1999)) of the unreddened SED for a single stellar population⁸. Dust emission in the IR is taken into account using 64 templates of Dale & Helou (2002). These models are parametrized by α , the power law slope of the dust mass over heating intensity, defined as follows:

$$dM_d(U) = U^{-\alpha} dU, \quad (3)$$

where $M_d(U)$ is the dust mass heated by a radiation field of intensity U .

Bolometric and dust luminosities (L_{bol} and L_{dust} respectively) are derived from all the basic parameters (see Noll *et al.* (2009)) and dust emission due to non-thermal sources such as AGN can also be added; the fraction f_{AGN} of dust luminosity L_{dust} (in L_\odot) due to an AGN is estimated using AGN templates from Siebenmorgen *et al.* (2004).

The spectral line correction due to interstellar gas is performed as in Noll *et al.* (2009): for the optical band, empirical line templates are taken from the Kinney *et al.* (1996) starburst spectra while for the UV we use templates derived from SEDs presented in Noll *et al.* (2004). A correction for the redshift-dependent absorption of the intergalactic medium shortward of the Ly α line is also included using the algorithm of Meiksin (2006).

2.3. Comparison with data

A grid of theoretical photometric fluxes is calculated at the redshift of the objects considered and a Bayesian analysis is performed through the calculation of the χ^2 of each model:

$$\chi^2(M_{\text{gal}}) = \sum_{i=1}^k \frac{(M_{\text{gal}} f_{\text{mod},i} - f_{\text{obs},i})^2}{\sigma_{\text{obs},i}^2} \equiv -2\ln(L); \quad (4)$$

here the galaxy mass M_{gal} (in M_\odot) is treated as a free parameter, $f_{\text{mod},i}$ and $f_{\text{obs},i}$ are the theoretical and experimental fluxes respectively, the statistical photometry errors are considered in the term $\sigma_{\text{obs},i}$ and L is the normalized likelihood function.

3. MCMC TECHNIQUE AND COSMOMC

In Bayesian inference, the posterior probability of the parameters ($\vec{\theta}$) of a model in the light of the observed data (\vec{d}) is given by:

$$P(\vec{\theta}|\vec{d}) = \frac{P(\vec{d}|\vec{\theta})P(\vec{\theta})}{P(\vec{d})}; \quad (5)$$

here $P(\vec{d}|\vec{\theta}) \equiv L(\vec{\theta})$ is the likelihood of the data given the model, $P(\vec{\theta})$ is the prior on the parameters, which quantifies our *a priori* knowledge of the parameters and $P(\vec{d})$ (called Evidence) is a normalization factor. In

⁷ The parameter f_V has been labelled f_{att} in some previous papers.

⁸ In its current version, CIGALE directly outputs the dust-free D4000 break, see Buat *et al.* (2011).

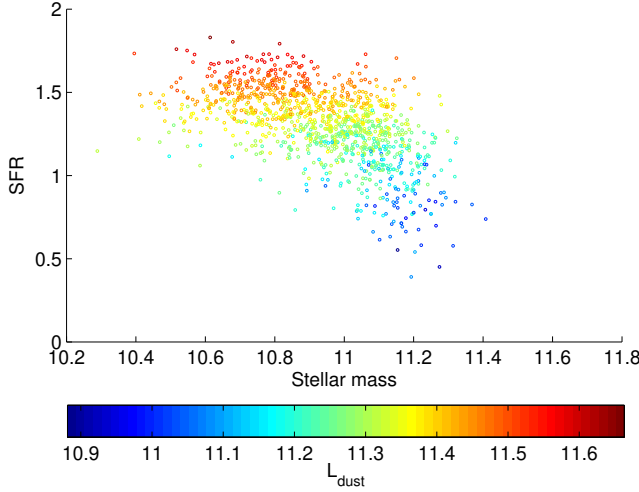


FIG. 1.— Samples from the posterior distribution for a test galaxy; the high density of points in the parameter space corresponds to large values of the posterior. Units are $M_{\odot}\text{yr}^{-1}$, M_{\odot} , L_{\odot} for SFR, M_{star} , L_{dust} respectively.

our case, \vec{d} represents the SED of each galaxy while $\vec{\theta}$ represents the astrophysical parameters of CIGALE, as $\{\theta\}_i \equiv \{\tau_1, t_2, f_{\text{ySP}}, \dots\}$. An MCMC sampler provides an efficient way to explore the posterior distribution and ensures that the number density of samples is asymptotically proportional to the probability density.

3.1. Metropolis-Hastings algorithm

The code `cosmomc` uses the Metropolis-Hastings algorithm to generate samples; each chain moves according to a transition probability $T(\vec{\theta}_i, \vec{\theta}_{i+1})$ which is determined so that the Markov Chain has a stationary asymptotic distribution equal to the posterior distribution $P(\vec{\theta})$ that we want to sample from. Given an arbitrary proposal density distribution $q(\vec{\theta}_i, \vec{\theta}_{i+1})$ to propose a new point $\vec{\theta}_{i+1}$ when the chain is at the point $\vec{\theta}_i$, the probability of transition is given by β :

$$\beta(\vec{\theta}_i, \vec{\theta}_{i+1}) = \min\left\{1, \frac{P(\vec{\theta}_{i+1})q(\vec{\theta}_{i+1}, \vec{\theta}_i)}{P(\vec{\theta}_i)q(\vec{\theta}_i, \vec{\theta}_{i+1})}\right\} \quad (6)$$

so that

$$T(\vec{\theta}_i, \vec{\theta}_{i+1}) = \beta(\vec{\theta}_i, \vec{\theta}_{i+1})q(\vec{\theta}_i, \vec{\theta}_{i+1}). \quad (7)$$

This ensures that the detailed balance holds:

$$P(\vec{\theta}_{i+1})T(\vec{\theta}_{i+1}, \vec{\theta}_i) = P(\vec{\theta}_i)T(\vec{\theta}_i, \vec{\theta}_{i+1}) \quad (8)$$

and that the distribution converges to $P(\vec{\theta})$. In practice, a random number $x \in [0 : 1]$ is generated in the process of moving from $\vec{\theta}_i$ to $\vec{\theta}_{i+1}$ so that the new point $\vec{\theta}_{i+1}$ is accepted if $\beta \geq x$. This ensures that each point of the chain depends only on its predecessor; in this sense the chain is a Monte-Carlo Markov process.

3.2. Comparison with grid-based methods, burn in and convergence diagnostics

As an illustration of the sampling mechanism, in Figure 1 we plot samples from the posterior distribution

for a MCMC run with a test galaxy taken from a mock sample at redshift $z \sim 0.7$ (see the following section for details); the number density of samples in the plane is proportional to the probability density of these two parameters. The dust luminosity L_{dust} strongly depends on the SFR and the two parameters are degenerate, as shown by the colours in the figure. This plot clearly shows the efficiency of this MCMC method. In the grid-based approach, the parameter space is sampled in the same “blind” way for high and low values of the posterior: this can be an issue for both reliability of results and computation time, as also pointed out in Noll et al. (2009) and Acquaviva et al. (2011). In fact, local minima and degeneracies between parameters can be easily missed or undersampled without a good a priori knowledge of the parameter space; the oversampling of an ill-constrained parameter can also lead to a slight degradation of the estimates of well constrained parameters and many points can be generated in a region where the posterior is low, resulting in a waste of CPU time. This is not the case when MCMC chains are used because each chain “learns” where to move in the parameter space through the Metropolis-Hastings algorithm so that the density of samples is proportional to the posterior distribution. Degeneracies between parameters are more easily found, especially if many chains, starting from different regions in the parameter space, are used. In other words, the CIGALEMC user needs to specify the prior parameter space (number of parameters and their limits) but not the density of points for each parameter. In the following section we will provide a comparison of CPU time between the original CIGALE and CIGALEMC when evaluating physical properties of a mock sample. The code also calculates the covariance between various parameters so that an initial run can be made and the covariance matrix obtained can be used to improve the efficiency of sampling for subsequent runs.

Since each MCMC chain starts at a random position in the parameter space, it will take a little time before the chain equilibrates and starts sampling the posterior distribution. This period of initial convergence is called *burn in* period and the first *burn in* points of each chains will be discarded when doing any statistical analysis. In order to obtain uncorrelated samples of the posterior each chain is also “thinned” by using only occasional points of it; the *thinning* factor varies according to the number of parameters involved and it is typically in the range 25-50. The code allows to choose the *burn in* fraction of the chain we want to discard and automatically thins out the chains.

In our analyses we won’t use any initial covariance matrix for the parameters and, in order to be conservative, we compute statistical quantities using only the second half of each chain. In Figure 2 we plot the points of a MCMC chain for a galaxy sample in the plane L_{dust} vs f_{AGN} ; the chain reaches the sensitive region of the parameter space after only a few “burn in” points characterized by very low values of L_{dust} . Having a set of samples from the full posterior distribution, it is possible to calculate statistical quantities for the parameters of interest. Since the number density of sampling points is proportional to the posterior density, it is easy to calculate mean values and marginalized 1-dimensional distribution for each parameter θ^i by simply counting the number N of samples

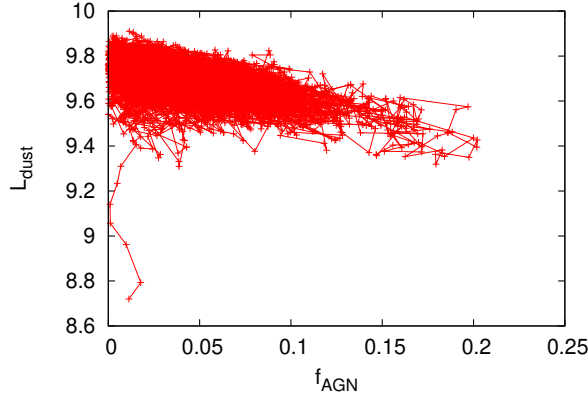


FIG. 2.— A Monte Carlo Markov chain in the 2-dimensional parameter space L_{dust} vs f_{AGN} . The chain starts in a region where the likelihood is low (“burn in” points with $L_{\text{dust}} \sim 8.8 L_{\odot}$) and quickly reaches the most sensitive region in the parameter space.

within binned ranges of parameter values:

$$\langle \theta^i \rangle \sim \frac{1}{N} \sum_{j=1}^N \theta_j^i, \quad (9)$$

while this is much more difficult in the context of the numerical grid integration because the calculation time grows exponentially with the number of dimensions. In order to be sure that MCMC chains are efficiently sampling the posterior distribution (and then obtain robust statistics for each parameter) it is important to check their convergence. The code *cosmomc* provides two convergence criteria for runs with one single chain (Raftery & Lewis, 1992) and with multiple chains (Gelman & Rubin, 1992). In the following analysis we will run multiple chains using the Gelman & Rubin diagnostic which is characterized by the “variance of chain means”/“mean of chain variances” parameter R ; $|R - 1| \leq 0.03$ is usually enough to reach convergence and stop the chains. In this work we use *cosmomc* as a generic MCMC sampler and we link it to *CIGALE* in order to allow a faster exploration of the astrophysical parameter space. Our modified *CIGALEMC* code will be publicly available very soon⁹ and, since it is based on *cosmomc* for sampling options, convergence criteria and statistical quantities provided, we refer the reader to the website¹⁰ and to Lewis & Bridle (2002) and references therein for a detailed explanation of the code and MCMC methods in general.

4. ANALYSIS OF A MOCK SAMPLE

We test our *CIGALEMC* code with a mock sample already used in Giovannoli *et al.* (2011). We consider 62 artificial galaxy SEDs corresponding to Luminous InfraRed Galaxies (LIRGs) at redshift $z \sim 0.7$ and obtained by varying the input parameters of *CIGALE* in the following ranges: $[0.1 \text{ Gyr} \leq \tau_1 \leq 10 \text{ Gyr}, 0.025 \text{ Gyr} \leq t_2 \leq 0.7 \text{ Gyr}, 0 \leq f_{\text{ySP}} \leq 1, 0.6 \text{ mag} \leq A_{\text{ySP}} \leq 2.1 \text{ mag}, 0 \leq f_V \leq 1, 1.0 \leq \alpha \leq 2.5, 0 \leq f_{\text{AGN}} \leq 0.3]$; such a wide multidimensional parameter space allows to model very different spectral energy distributions of galaxies charac-

terized by a wide range of possible star formation histories, absorption and emission by gas and dust and AGN contamination. All galaxies are based on a Salpeter initial mass function; the age of the old stellar population is fixed at 7 Gyr, we consider a constant star formation rate for the young population model ($\tau_2 = 20$ Gyr) and we do not add any modification to the original Calzetti attenuation curve (no UV bump and $\delta = 0$).

Theoretical fluxes are calculated in the following 17 bands from UV to IR: $0.231 \mu\text{m}$ for GALEX, $[0.35 - 0.36 - 0.46 - 0.54 - 0.65 - 0.87 - 0.90 - 1.2 - 1.6 - 2.1] \mu\text{m}$ (corresponding to MUSYC bands), $[3.6 - 4.5 - 5.8 - 8.0] \mu\text{m}$ (corresponding to IRAC photometry) and $[24 - 70] \mu\text{m}$ (corresponding to MIPS photometry). We add a gaussian distributed uncertainty σ to each theoretical flux; its value is 10% of the corresponding flux, a reasonable choice for the measurements considered above. For each galaxy we run 8 chains with initial positions randomly chosen in the parameter space determined by the following set of input parameters:

$$\{\tau_1, t_2, f_{\text{ySP}}, A_{\text{ySP}}, f_V, \alpha, f_{\text{AGN}}, M_{\text{gal}}\}. \quad (10)$$

from which statistical quantities of interest can be calculated for the following set of derived parameters :

$$\{\text{SFR}, t_{\text{D4000}}, L_{\text{bol}}, L_{\text{dust}}, A_{\text{FUV}}, A_V, M_{\text{star}}\}. \quad (11)$$

We assume flat priors in the following parameters space: $[0.1 \text{ Gyr} \leq \tau_1 \leq 10 \text{ Gyr}, 0.025 \text{ Gyr} \leq t_2 \leq 2 \text{ Gyr}, 0 \leq f_{\text{ySP}} \leq 1, 0 \text{ mag} \leq A_{\text{ySP}} \leq 3 \text{ mag}, 0 \leq f_V \leq 1, 0.5 \leq \alpha \leq 3, 0 \leq f_{\text{AGN}} \leq 1, 8 M_{\odot} < M_{\text{gal}} < 14 M_{\odot}]$; chains are stopped when the Gelman & Rubin R -1 parameter is $|R - 1| \sim 0.03$.

First of all, we want to check that our results are statistically in agreement with the input values for the mock sample. As a tool derived from *cosmomc*, *CIGALEMC* allows to calculate and plot the mean likelihood and marginalized distribution for each parameter.

The marginalized distribution in a given direction of the parameter space $\vec{d} = \mathbf{h}(\vec{\theta})$ (where $\mathbf{h}(\vec{\theta})$ is the projector operator in one of the parameters considered, as $\mathbf{h}(\vec{\theta}) = \theta_i$) is proportional to the number of samples at \vec{d} and it can be expressed as:

$$P(\vec{v}) = M(P, \vec{v}) \equiv \int d\vec{\theta} P(\vec{\theta}) \delta(\mathbf{h}(\vec{\theta}) - \vec{v}), \quad (12)$$

where $P(\vec{\theta})$ is the posterior distribution. Assuming flat priors on $\vec{\theta}$, the mean likelihood of samples with $\vec{d} = \mathbf{h}(\vec{\theta})$ can be expressed as:

$$\langle P(\vec{v} : \mathbf{h}(\vec{\theta}) = \vec{v}) \rangle \equiv \frac{\int d\vec{\theta} P(\vec{\theta})^2 \delta(\mathbf{h}(\vec{\theta}) - \vec{v})}{\int d\vec{\theta} P(\vec{\theta}) \delta(\mathbf{h}(\vec{\theta}) - \vec{v})} = \frac{M(P^2, \vec{v})}{M(P, \vec{v})}. \quad (13)$$

If $P(\vec{\theta})$ is a multivariate Gaussian distribution it is possible to demonstrate that both mean likelihood and marginalized distribution are Gaussian and proportional so that they look the same: differences in these distributions will be then a signal of non-Gaussianity which can be either intrinsic or due to parameters not very well constrained. In Figure 3 we show, for an artificial galaxy of the mock sample considered, both marginalized distributions (black solid lines) and mean likelihood (dotted lines) for some parameters of interest: we can see that

⁹ <http://www.oamp.fr/cigale/>.

¹⁰ <http://cosmologist.info/cosmomc/>

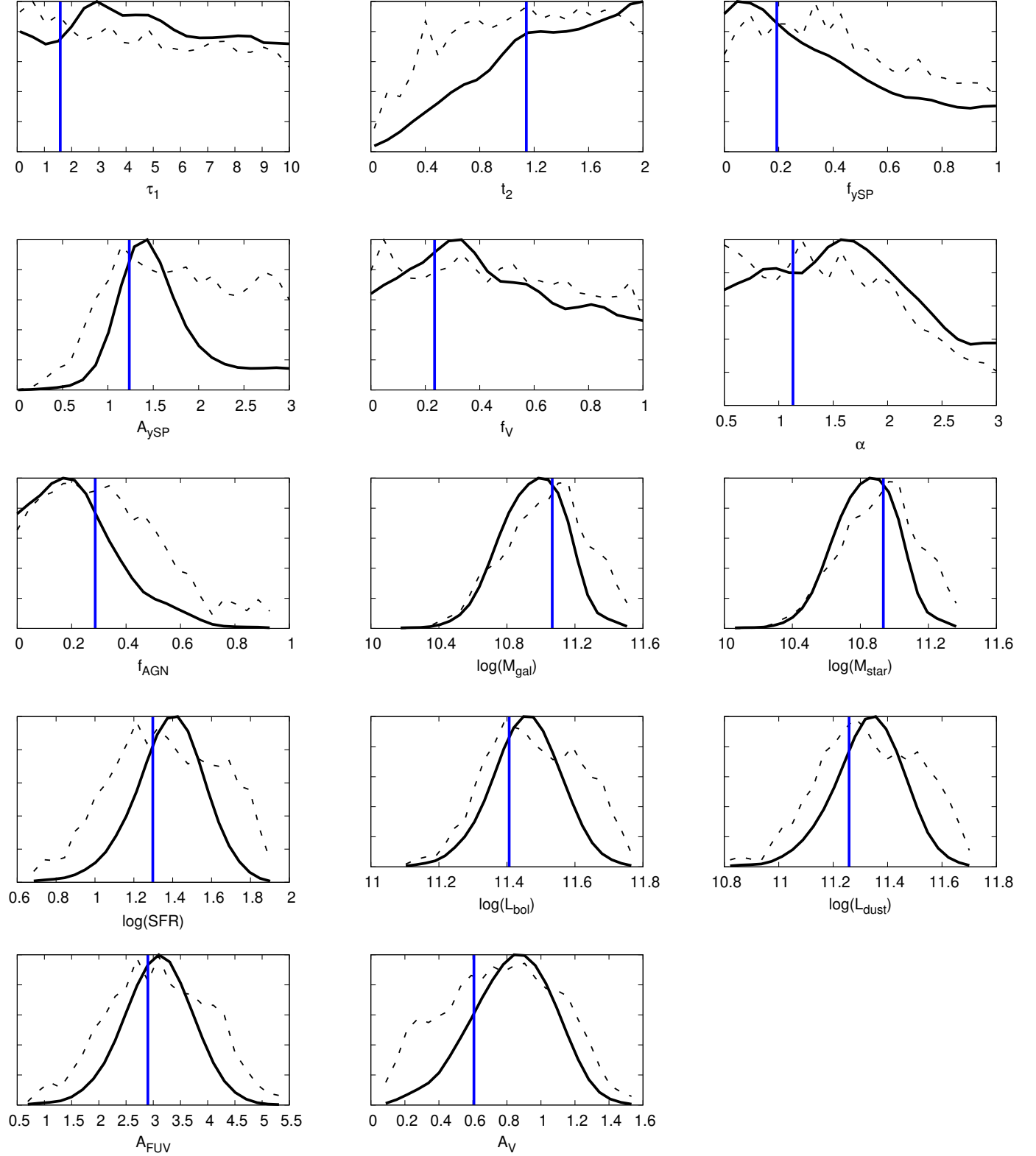


FIG. 3.— Mean likelihoods, computed over the whole chains, for binned parameter values (dotted lines) and marginalized distributions (black lines) of some parameters of interest for an artificial galaxy of the mock sample considered; the blue vertical lines show the input parameter values used. Poorly constrained parameters, such as τ_1 , t_2 , f_{ySP} , f_V and α are clearly visible. Luminosities and masses are in units of solar luminosities and solar masses respectively.

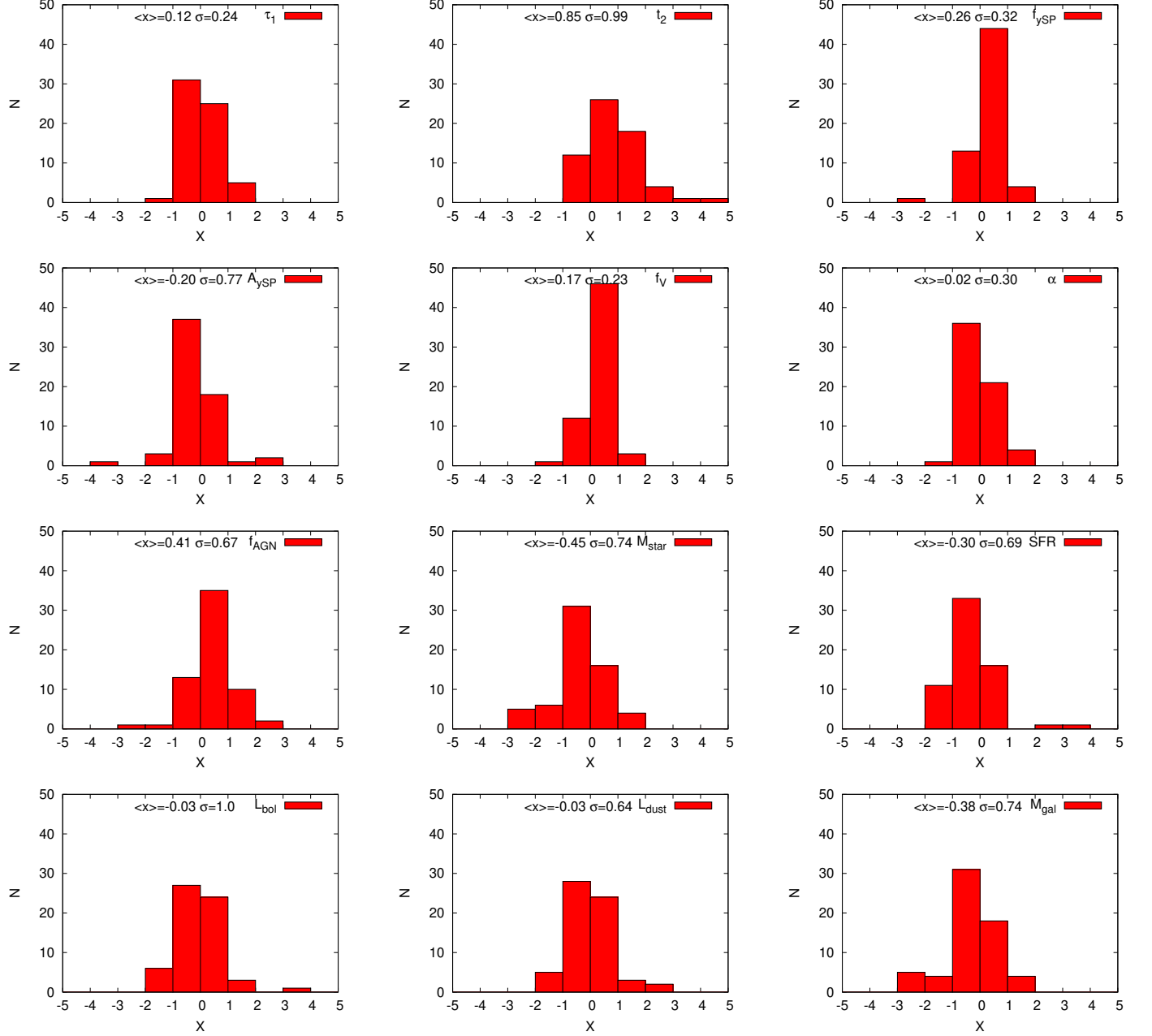


FIG. 4.— Distribution of the variable X for some parameters considered; X values are compatible with 0 at 68% c.l..

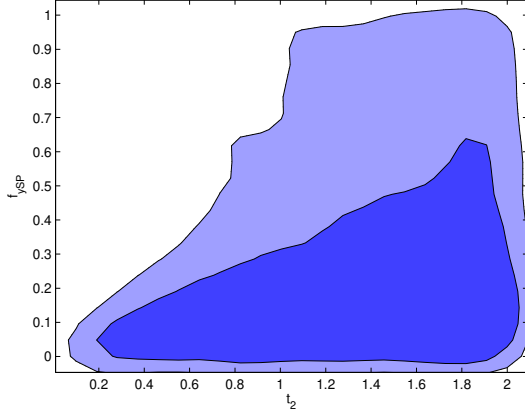


FIG. 5.— Two-dimensional marginalized distribution showing the 68% and %95 c.l. contours for f_{ySP} and t_2 for a galaxy sample; the parameter t_2 is unconstrained by the data and it is partially degenerate with f_{ySP}

τ_1 , t_2 , f_{ySP} , f_V and α are not very well constrained by the code. Similar results have been found in the analyses by Noll et al. (2009), Giovannoli et al. (2011) and Buat et al. (2011).

In order to study the goodness of the fit in a quantitative way for the whole sample of galaxies we introduce the quantity:

$$X^i \equiv \frac{1}{N} \sum_j \frac{O_j^i - I_j^i}{\sigma_j^i}; \quad (14)$$

here i runs for all the parameters considered by the code (so that $\{X\}^i = \{\tau_1, t_2, f_{ySP}, \dots\}$), j runs for the $N = 62$ objects of the mock, O_j^i is the set of the best fit values obtained as output from CIGALEMC, I_j^i is the vector of input parameters and σ_j^i is the vector of the 68% c.l. marginalized uncertainties. As we can see from Figure 4, all X values are compatible with $X = 0$, which means that the code is able to find the best fit values of the parameters with high confidence. However, some distributions are slightly skewed: this can be due to chains being stuck in local minima of the likelihood function so that, in some cases, the best fit found does not correspond to the input value. This situation is typical when parameters are not well constrained (as for t_2) or in the presence of strong degeneracies between parameters. As an example, Figure 5 shows the 68% and 95% c.l. in the plane f_{ySP} vs t_2 for one sample galaxy of the mock: as we can see, limits on these parameters are not very strong; we also notice a partial degeneracy for high values of f_{ySP} which is due to the fact that these two parameters affect the galactic SFR in the same way since we consider constant SFR for the young model:

$$\text{SFR} \sim f_{ySP} \frac{M_{\text{gal}}}{t_2}. \quad (15)$$

In order to check the reliability of our MCMC algorithm we tested the parameter uncertainty estimation. We created and fit the SEDs of 100 artificial galaxies in 21 bands from IR to UV, built with the same input parameter set and with a 10% scatter in flux, corresponding to the photometric error considered. We checked that in

Parameters	mock sample
τ_1	0.33
$\log_{10} M_{\text{star}}$	0.93
$\log_{10} L_{\text{bol}}$	0.92
$\log_{10} L_{\text{dust}}$	0.88
$\log_{10} \text{SFR}$	0.81
t_2	0.26
f_{ySP}	0.30
A_{ySP}	0.81
f_V	0.70
α	0.65
f_{AGN}	0.71

TABLE 1
ESTIMATION OF THE LINEAR CORRELATION COEFFICIENT OF PEARSON BETWEEN THE EXACT VALUE AND THE VALUE ESTIMATED BY THE CODE CIGALEMC FOR SOME PARAMETERS OF THE MOCK CATALOGUE.

general we are able to find the true values within the region allowed at 68 (95)% confidence 68 (95)% of the time within the Poisson fluctuation error for different choices for both the input parameters and the prior ranges allowed in the fit.

Finally, we checked the consistency of our results by calculating the Pearson correlation coefficient r between the input values of the parameters used to generate the mock and the best fit values found with CIGALEMC. The Pearson correlation coefficient quantifies the amount of correlation between two variables X and Y and it assumes values in the range $r \in [-1 : 1]$ (see Cohen (1988)). For samples X_i and Y_i , it can be written as:

$$r = \frac{\sum_{i=1}^N (X_i - \bar{X})(Y_i - \bar{Y})}{(\sum_{i=1}^N (X_i - \bar{X})^2)^{\frac{1}{2}} (\sum_{i=1}^N (Y_i - \bar{Y})^2)^{\frac{1}{2}}}; \quad (16)$$

here \bar{X} and \bar{Y} denote the mean values of X_i and Y_i . The interpretation of the strength of the correlation can depend on the context; however, a widely used standard introduced by Cohen (1988) considers Pearson values $|r| > 0.5$ as a signal of large correlation between variables, while $|r| < 0.3$ denotes poor correlation. Again, as we can see from Table 1, some parameters (τ_1 , t_2 , f_{ySP}) have small values of r ; this is expected since these parameters are mostly unconstrained; however, even if the exact values of the input parameters are not found, they always fall inside the statistically significant region of the parameter space. We also explicitly checked that results do not significantly change when increasing the prior space for some parameters not very well constrained as τ_1 , t_2 and α . Finally, we tested, for a galaxy of the mock, how results change when considering a gaussian prior, with different central values and width $\sigma = 0.2$, on one of the most unconstrained parameters, t_2 ; we found that results on the other parameters are always statistically consistent respect to the choice of a flat prior on t_2 . In general, it is a good idea to choose the largest possible prior space for unconstrained parameters, in order to avoid possible biases due to the prior choice.

It is useful to compare the performance of CIGALE and CIGALEMC in terms of computing time, especially since computation can become prohibitive for any grid-based method if the number of parameters involved is sufficiently high. The CPU time required to obtain convergence of the chains for each galaxy mainly depends on

both the quality of the data and the number of parameters considered. Running 8 chains in parallel (each one on a 2.40 GHz Intel Xeon E5530), for each galaxy of the mock we typically reach a good convergence with ~ 20000 points for each chain, which means a total of ~ 160000 points. The grid built in Giovannoli *et al.* (2011) to analyze the same sample with the same number of free parameters and bounds contained $\sim 3.5 \cdot 10^6$ points; this means a gain of order ~ 20 in efficiency in the estimation of the parameters but a more dramatic efficiency can be easily reached when we need to use either more parameters or a fine sampling in a given direction of the parameter space or both. The average CPU time to reach a good convergence for a galaxy of this mock is about 35 seconds, which translates in 280s of total CPU time.

5. ANALYSIS OF REAL DATA: THE SINGS SAMPLE

We now use CIGALEMC to infer physical properties of the well known SINGS (Spitzer Infrared Nearby Galaxy Survey; Kennicutt *et al.* (2003)) sample. In order to make a comparison with results obtained using the grid-based CIGALE, we use the same 39 galaxies already considered in Noll *et al.* (2009) with the same spectral coverage: GALEX FUV ($\sim 1500\text{\AA}$) and NUV ($\sim 2300\text{\AA}$) filters (Gil de Paz *et al.* (2007)), 2MASS data for J, H, K_s (Jarrett *et al.* (2003)), IRAC and MIPS filters for [3.6, 4.5, 5.8, 8.0, 24, 70, 160] μm (Dale *et al.* (2005)), Dale *et al.* (2007, 2008) optical data for B, V, R and I bands corrected as in Muñoz-Mateos *et al.* (2009) and fluxes from u' , g' , r' , i' and z' filters of SDSS (Stoughton *et al.* (2002)); Dale *et al.* (2007, 2008) optical data are only used for 14 galaxies for which SDSS data are not available. The mean photometric relative uncertainties for the bands considered are shown in Table 2; in particular, very small uncertainties are associated with the 2MASS bands. We performed a preliminar run, realizing that the hard constraints coming from this filter set did not allow the code to properly fit for the other filters. Since these uncertainties do not take into account for possible calibration errors and since a systematic offset can also affect the CIGALE theoretical models, we decided to be conservative and, following Noll *et al.* (2009), we add a 5% uncertainties in quadrature for each filter set.

In our analysis we assume the following range of vari-

Filters	Rel. errors
GALEX FUV, NUV	15%
Dale <i>et al.</i> B, V, R, I	16%
SDSS u , g , r , i , z	3%
2MASS J, H, K _s	1%
IRAC 3.6, 4.5, 5.8, 8.0 μm	11%
MIPS 24 μm	5%
MIPS 70 μm	7%
MIPS 160 μm	13%

TABLE 2

MEAN PHOTOMETRIC UNCERTAINTIES FOR OUR SINGS SAMPLE.

ation for a set of 9 astrophysical parameters: $[0.1 \text{ Gyr} \leq \tau_1 \leq 10 \text{ Gyr}, 0.025 \text{ Gyr} \leq t_2 \leq 2 \text{ Gyr}, 0 \leq f_{ySP} \leq 1, -0.5 \leq \delta \leq 0.5, 0 \text{ mag} \leq A_{ySP} \leq 5 \text{ mag}, 0 \leq f_V \leq 1, 0.5 \leq \alpha \leq 3, 0 \leq f_{AGN} \leq 1, 8M_\odot, M_{\text{gal}} < 13M_\odot]$. We keep fixed both the age of the old stellar population

($t_1 = 10 \text{ Gyr}$) and the e-folding time for the young stellar population ($\tau_2 = 20 \text{ Gyr}$): these parameters are not well constrained by the data so that fixing them does not alter the fit. Finally, We only consider models with Salpeter initial mass function and solar metallicity; metallicity measurements are quite uncertain due to many limiting factors (Noll *et al.* (2009), Moustakas & Kennicutt (2006) and references therein); Noll *et al.* (2009) checked the influence of different assumptions for the metallicity, concluding that deviations in the properties of the galaxies are within the uncertainties, which tend to increase by 0 to 20% when half or double of the solar metallicity are considered. The only exception is the absolute value of t_{D4000} , because of the well-known age-metallicity degeneracy (e.g., Kodama & Arimoto, (1997)).

Our reference AGN model has $L = 10^{12} L_\odot$, $R = 125 \text{ pc}$ and $A_V = 32$ for the luminosity of the non-thermal source, the outer radius of a spherical dust cloud covering the AGN and the amount of attenuation in the optical caused by the cloud respectively.

Our findings can be summarized as follows:

- Very good constraints are derived for the AGN fraction of all sources ($f_{AGN} \leq 0.10$) except for NGC0584 and NGC1404 for which $f_{AGN} \leq 0.6$ at 68% c.l.. We note that the flux at $160\mu\text{m}$ for NGC0584 can be contaminated by some foreground/background emission and the most recent Herschel data conclusively confirm that a background source contaminates both fluxes at 70 and $160\mu\text{m}$ for NGC1404 (Daniel Dale, private communication); the low quality of these data is responsible for the big uncertainties obtained for other parameters as $\text{SFR } L_{\text{bol}} L_{\text{dust}} A_{\text{FUV}}$; in Figure 6 we plot the 2-dimensional marginalized distribution for SFR vs f_{AGN} for NGC1404: the double-peaked likelihood function is most probably an artifact due to the low quality of data for this source. In general, we note that that NGC0584 and NGC1404 are elliptical galaxies which tend to have very weak but warm dust emission; it is not surprising that they show an apparently high AGN fraction. We decided not to use these sources in the rest of our analysis.
- We are not able to put strong constraints on “phenomenological” parameters as τ_1 , t_2 and δ ; limits on these parameters depend on the assumed prior range. The poor determination of δ is essentially due to the low number of data in UV. In general, both δ and the possible UV bump allowed by the code are very difficult to constrain with few only broad band data (Buat *et al.* (2011) and Buat *et al.*, in preparation). The fraction of the young stellar mass over the total mass is well constrained, with values $f_{ySP} < 0.26$ for all the galaxies, except for NGC1705, NGC2798 and NGC4631, for which f_{ySP} is unconstrained. The mean value for the parameter α of the Dale & Helou (2002) templates is $\alpha = 2.44$ (in agreement with Noll *et al.* (2009); we note that, while low values of α are well constrained, no constraints are found on high values, with $\alpha = 3$ compatible at 68% c.l. for all galaxies except NGC2798, for which $\alpha < 1.77$ at 68% c.l.; weak constraints on high values for α are due to the

degeneracy of the dust emission models for wavelengths shortwards of the emission peak, so that, for $\alpha > 2.5$, the flux ratio $f_\nu(60\mu m)/f_\nu(100\mu m)$ is almost constant (see Noll et al. (2009)).

- Good constraints can be derived for the mass dependent parameters M_{star} , SFR, L_{bol} and L_{dust} as shown in Table 3. The Pearson correlation coefficient with results from Noll et al. (2009) is $r = 0.99, 0.98, 0.94, 1.0, 1.0, 0.94$ for M_{star} , SFR, t_{D4000} , L_{bol} , L_{dust} , A_{FUV} respectively. In Figure 8 we show a quantitative comparison with the analysis performed by Noll et al. (2009) with the original code CIGALE by plotting the ratio, $Q \equiv (\text{CIGALEMC} - \text{CIGALE})/\sigma_{\text{CIGALEMC}}$, where CIGALEMC and CIGALE refer to the mean value of the parameters quoted in Table 3 for this work and Noll et al. (2009) respectively. Possible systematic differences between the results of both methods can be studied by considering mean, standard deviation and skewness for the parameters of interest. As we can see from Table 4, no significant difference between results in this paper and in Noll et al. (2009) is found for SFR, $\log(t_{\text{D4000}})$, $\log(L_{\text{bol}})$, and A_{FUV} , with each value compatible with 0 at less or about 68% c.l.; however, there is some skewness associated to SFR, t_{D4000} and L_{bol} . In case of M_{star} and L_{dust} , the mean values are lower from 0 at about 95% c.l., indicating the existence of some offset between results in this paper and in Noll et al. (2009). A further comparison of the uncertainties between our results and Noll et al. (2009) shows that we are able to put stronger constraints on the galaxy SFR, while our constraints on M_{star} , L_{bol} , L_{dust} , A_{FUV} are weaker. Differences between our results and results in Noll et al. (2009) can be due to the different choice of the input parameter space in terms of both number and type of parameters used in the analysis; in particular, we consider a wider range of variation for α , δ , A_{ySP} , t_2 and f_{AGN} , while we decide to fix the parameter τ_2 (see Table 3 of Noll et al. (2009) for their choice of the parameter space); however, it is reassuring to see how different theoretical assumptions lead to compatible results.

- A frequency dependent χ^2 analysis shows which bands mostly contribute to the total χ^2 for each galaxy. We introduce the averaged χ^2 :

$$\langle \chi^2(\lambda^j) \rangle = \frac{1}{N_j} \sum_{i=1}^{N_j} \left(\frac{\text{Th}_i^j - d_i^j}{\sigma_i^j} \right)^2; \quad (17)$$

here Th_i^j and d_i^j are respectively the theoretical best fit SEDs and the data points for the i -th galaxies at the j -th frequency and the sum runs over our sample of galaxies. From Figure 7 we see that the code is able to find a good agreement with the data for all the bands considered. The frequency dependent χ^2 is particularly low for bands with large relative errors as UV GALEX bands and optical B, V, R, I bands. The large uncertainty found for the MIPS $70\mu m$ filter is mainly due to the galaxies NGC1715 and NGC5866; the code is not able to find a good fit for the $70\mu m$ filter and the reduced chi-squared

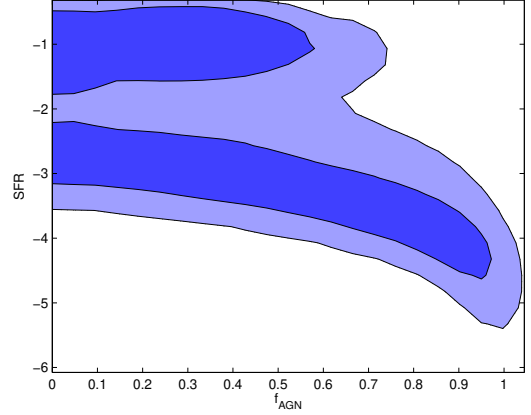


FIG. 6.— Two-dimensional marginalized distribution showing the 68% and 95% c.l. contours for $\log(\text{SFR})$ vs f_{AGN} for NGC1404; the double peaked likelihood is clearly visible and f_{AGN} is mostly unconstrained.

is high ($\chi^2/d.o.f = 7.8$ for both galaxies, see Table 3). A previous analysis by Cannon et al. (2006), based on Spitzer observations, found similar results for NGC1705, showing in particular that the models of Li & Draine (2001, 2002) give a better fit to IR data than the Dale & Helou (2002) models used in this paper (see Figure 3 of Cannon et al. (2006)). Interestingly enough, NGC1715 and NGC5866 are, respectively, the only irregular and S0 galaxies in our sample.

In general, we find a small trend of worse fitting for galaxies with small SFR values. Galaxies with the lowest values of the χ^2 do not show peculiar properties, with total stellar masses of about $10^{11} M_\odot$ and SFRs between 0.1 and $10 M_\odot/\text{yr}$, typical of nearby spiral galaxies; an exception is the dwarf galaxy NGC4625 (reduced $\chi^2/d.o.f = 1.2$), characterized by smaller values for both the stellar mass and luminosity. Three other dwarf galaxies (NGC1705, NGC2976 and NGC5474) are clearly identified in our sample by looking at their smaller values for both the luminosity and the stellar masses respect to the rest of the sample. Finally, in order to check for a possible correlation between the filter set used and the goodness of the fit, we also calculated the mean χ^2 for the subset of galaxies for which SDSS filters are available respect to the subset of galaxies with optical Dale et al. filters; we found no correlation, with $\bar{\chi} \sim 2.5$ in both cases.

6. CONCLUSIONS

In this paper we have introduced a MCMC sampling method for the astrophysical parameter estimation from SED fitting with CIGALE. We have shown the following advantages of our modified CIGALEMC code over the usual grid-based CIGALE:

- its efficiency, in terms of CPU time, through the Metropolis-Hastings algorithm. Most of the sampling points are drawn in the region where the posterior probability is high, while in the grid-based approach all regions are sampled in the same way.

TABLE 3
MEAN VALUES AND 68% C.L. MARGINALIZED RESULTS FOR SOME PARAMETERS RELATED TO THE SINGS SAMPLE CONSIDERED.

ID	Type	$\log M_{\text{star}}$ [M_{\odot}]	$\log \text{SFR}$ [M_{\odot}/yr]	$\log t_{\text{D4000}}$ [Gyr]	$\log L_{\text{bol}}$ [L_{\odot}]	$\log L_{\text{dust}}$ [L_{\odot}]	A_{FUV} [mag]	$\chi^2/\text{d.o.f.}$
NGC 0024	SAc	9.52 ± 0.10	-0.78 ± 0.11	-0.14 ± 0.18	9.46 ± 0.05	8.62 ± 0.11	0.45 ± 0.16	2.5
NGC 0584	E4	11.41 ± 0.04	-1.3 ± 0.25	0.99 ± 0.02	11.09 ± 0.18	10.22 ± 1.14	4.47 ± 4.41	2.7
NGC 0925	SABd	9.93 ± 0.17	0.18 ± 0.12	-0.43 ± 0.10	10.24 ± 0.07	9.64 ± 0.09	0.6 ± 0.21	2.6
NGC 1097	SBb	11.19 ± 0.11	0.9 ± 0.11	-0.15 ± 0.17	11.15 ± 0.04	10.77 ± 0.08	1.85 ± 0.51	0.5
NGC 1291	SBa	11.14 ± 0.05	-0.72 ± 0.23	0.86 ± 0.08	10.68 ± 0.04	9.24 ± 0.16	0.98 ± 0.66	1.9
NGC 1316	SAB0	12.01 ± 0.05	-0.06 ± 0.28	0.91 ± 0.07	11.54 ± 0.04	10.07 ± 0.12	1.49 ± 1.07	4.5
NGC 1404	E1	11.52 ± 0.04	-1.0 ± 0.20	0.98 ± 0.02	11.25 ± 0.21	10.76 ± 0.58	5.58 ± 5.07	1.4
NGC 1512	SBab	10.34 ± 0.09	-0.28 ± 0.14	0.17 ± 0.32	10.13 ± 0.04	9.39 ± 0.09	0.86 ± 0.30	1.8
NGC 1566	SABbc	10.88 ± 0.11	0.9 ± 0.10	-0.34 ± 0.08	11.02 ± 0.05	10.58 ± 0.08	1.13 ± 0.34	1.6
NGC 1705	Am	8.20 ± 0.20	-1.15 ± 0.15	-0.62 ± 0.25	8.81 ± 0.10	7.67 ± 0.12	0.11 ± 0.05	7.8
NGC 2798	SBa	10.03 ± 0.18	0.61 ± 0.07	-0.54 ± 0.06	10.6 ± 0.05	10.47 ± 0.06	4.48 ± 0.64	2.0
NGC 2841	SAb	10.92 ± 0.06	-0.3 ± 0.17	0.62 ± 0.10	10.54 ± 0.03	9.57 ± 0.11	1.04 ± 0.46	1.3
NGC 2976	SAc	9.33 ± 0.09	-0.8 ± 0.08	-0.28 ± 0.06	9.37 ± 0.04	8.87 ± 0.09	1.11 ± 0.28	3.4
NGC 3031	SAab	10.96 ± 0.06	-0.16 ± 0.14	0.56 ± 0.10	10.59 ± 0.03	9.51 ± 0.11	0.63 ± 0.27	1.8
NGC 3184	SABcd	10.14 ± 0.08	0.11 ± 0.07	-0.33 ± 0.07	10.24 ± 0.03	9.68 ± 0.09	0.78 ± 0.23	4.4
NGC 3190	SAap	10.87 ± 0.04	-0.65 ± 0.35	0.75 ± 0.15	10.44 ± 0.03	9.62 ± 0.10	3.16 ± 1.23	1.4
NGC 3198	SBc	10.01 ± 0.08	-0.02 ± 0.07	-0.33 ± 0.07	10.12 ± 0.04	9.55 ± 0.09	0.73 ± 0.21	2.2
NGC 3351	SBb	10.58 ± 0.08	-0.02 ± 0.12	0.14 ± 0.23	10.38 ± 0.04	9.82 ± 0.09	1.36 ± 0.41	1.1
NGC 3521	SABbc	10.95 ± 0.08	0.41 ± 0.14	0.06 ± 0.23	10.76 ± 0.04	10.28 ± 0.10	2.06 ± 0.51	0.9
NGC 3621	SAd	10.04 ± 0.12	0.14 ± 0.10	-0.38 ± 0.08	10.24 ± 0.05	9.82 ± 0.09	1.15 ± 0.35	1.4
NGC 3627	SABb	10.80 ± 0.10	0.55 ± 0.11	-0.21 ± 0.08	10.77 ± 0.04	10.38 ± 0.09	2.0 ± 0.40	1.7
NGC 4536	SABbc	10.89 ± 0.12	1.0 ± 0.10	-0.39 ± 0.08	11.11 ± 0.04	10.79 ± 0.08	1.65 ± 0.40	1.2
NGC 4559	SABcd	10.11 ± 0.16	0.43 ± 0.08	-0.47 ± 0.06	10.46 ± 0.04	9.84 ± 0.09	0.52 ± 0.15	3.3
NGC 4569	SABab	11.38 ± 0.05	0.33 ± 0.17	0.53 ± 0.12	11.03 ± 0.03	10.26 ± 0.10	1.66 ± 0.56	4.0
NGC 4579	SABb	11.42 ± 0.06	0.18 ± 0.21	0.63 ± 0.11	11.03 ± 0.03	10.13 ± 0.11	1.5 ± 0.60	1.3
NGC 4594	SAa	11.73 ± 0.05	-0.44 ± 0.27	0.94 ± 0.06	11.26 ± 0.04	9.7 ± 0.12	1.29 ± 0.97	1.4
NGC 4625	SABmp	9.18 ± 0.10	-0.77 ± 0.08	-0.37 ± 0.08	9.33 ± 0.04	8.79 ± 0.10	0.75 ± 0.22	1.2
NGC 4631	SBd	10.08 ± 0.17	0.76 ± 0.07	-0.59 ± 0.06	10.73 ± 0.04	10.45 ± 0.08	1.39 ± 0.36	2.9
NGC 4725	SABab	11.34 ± 0.07	0.31 ± 0.15	0.51 ± 0.11	11.0 ± 0.03	10.01 ± 0.12	0.7 ± 0.29	2.3
NGC 4736	SAab	10.75 ± 0.07	0.08 ± 0.12	0.21 ± 0.30	10.51 ± 0.03	9.84 ± 0.10	1.2 ± 0.36	1.7
NGC 4826	SAab	10.77 ± 0.05	-0.44 ± 0.21	0.62 ± 0.12	10.38 ± 0.03	9.54 ± 0.11	1.78 ± 0.68	2.6
NGC 5033	SAc	10.68 ± 0.10	0.43 ± 0.11	-0.20 ± 0.09	10.65 ± 0.04	10.25 ± 0.09	1.7 ± 0.42	1.2
NGC 5055	SAbc	10.88 ± 0.08	0.45 ± 0.11	-0.06 ± 0.14	10.75 ± 0.04	10.27 ± 0.09	1.7 ± 0.41	2.2
NGC 5194	SABbc	10.74 ± 0.11	0.85 ± 0.09	-0.39 ± 0.08	10.94 ± 0.04	10.55 ± 0.09	1.3 ± 0.33	0.8
NGC 5195	SB0p	10.76 ± 0.04	-0.42 ± 0.27	0.61 ± 0.15	10.38 ± 0.04	9.61 ± 0.15	2.55 ± 0.92	5.6
NGC 5474	SACd	9.22 ± 0.14	-0.53 ± 0.10	-0.43 ± 0.07	9.52 ± 0.04	8.52 ± 0.12	0.19 ± 0.07	5.6
NGC 5713	SABbcp	10.54 ± 0.19	0.83 ± 0.11	-0.44 ± 0.09	10.89 ± 0.05	10.68 ± 0.08	2.74 ± 0.56	1.1
NGC 5866	S0	10.88 ± 0.04	-1.01 ± 0.36	0.87 ± 0.10	10.42 ± 0.03	9.2 ± 0.14	2.56 ± 1.26	7.8
NGC 7331	SAb	11.31 ± 0.11	0.78 ± 0.15	0.08 ± 0.32	11.13 ± 0.04	10.73 ± 0.09	2.62 ± 0.64	1.2

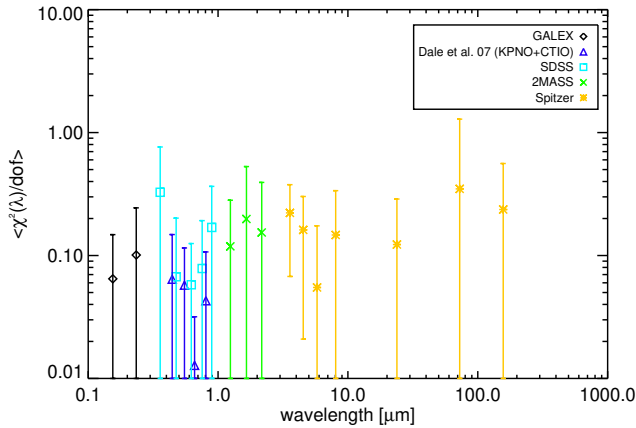


FIG. 7.— The averaged frequency dependent χ^2 for our SINGS sample shows a general good fit for all the bands used; the large dispersion for the $70\mu\text{m}$ MIPS filter is mainly due to NGC1705 and NGC5866. Error bars are calculated as standard deviations.

Parameters	mean	$\sqrt{\text{Var}}$	Skewness
$\log_{10} M_{\text{star}}$	-1.0	0.52	-0.1
$\log_{10} \text{SFR}$	0.29	0.89	1.79
$\log t_{\text{D4000}}$	1.2	2.8	2.6
$\log_{10} L_{\text{bol}}$	-0.45	0.36	1.17
$\log_{10} L_{\text{dust}}$	-0.58	0.25	0.01
A_{FUV}	-0.69	0.62	-0.25

TABLE 4
VALUES OF THE FIRST THREE MOMENTS OF THE $Q \equiv (\text{CIGALEMC} - \text{CIGALE})/\sigma_{\text{CIGALEMC}}$ DISTRIBUTIONS FOR SOME PARAMETERS OF INTEREST.

Moreover, marginalized one-dimensional probability distributions for the parameters of interest are calculated by simply counting the number of samples within a binned range of parameter values, the density of sampling points being proportional to the posterior probability. It is hard to do the same with the usual grid approach, since the integration calculation scales exponentially with the number of dimensions. The analysis of a mock

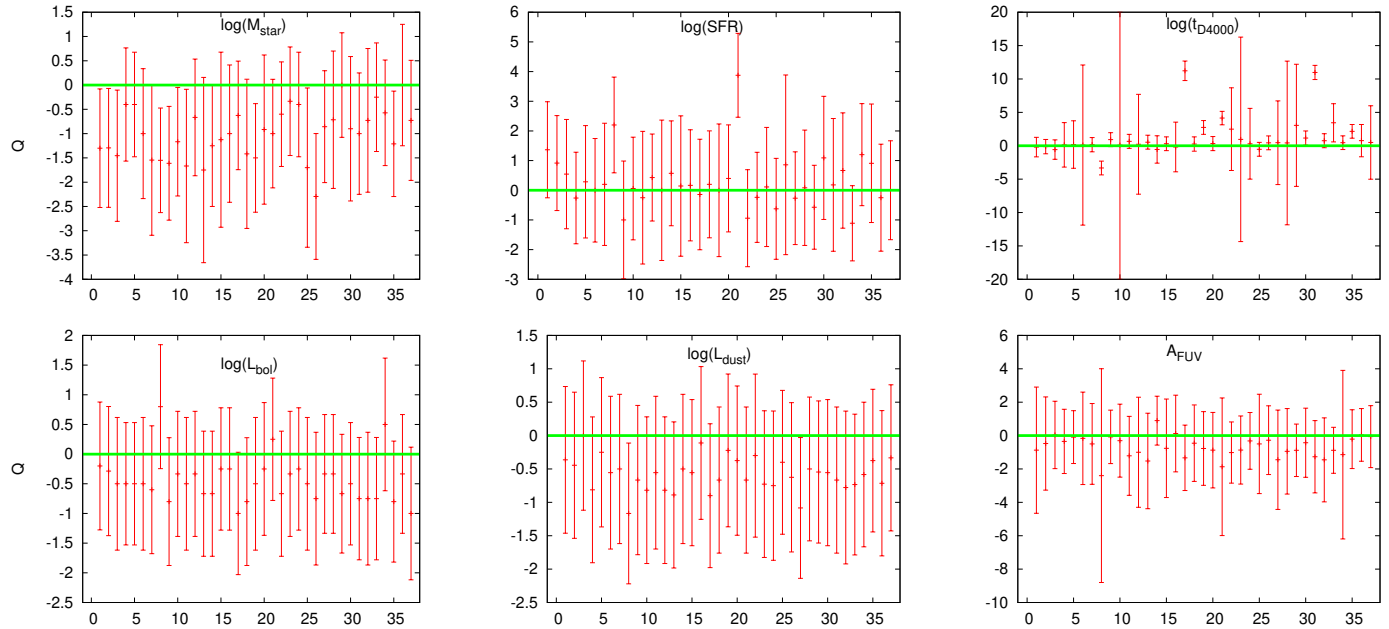


FIG. 8.— Ratio $Q \equiv (\text{CIGALEMC} - \text{CIGALE})/\sigma_{\text{CIGALEMC}}$ between the mean values estimated in this work and in Noll et al. (2009) for some parameters quoted in Table 3.

sample shows that **CIGALEMC** needs 20 times less points than **CIGALE** to reach convergence for a given galaxy but, in general, results depend on both the number of parameters and the prior used.

- its accuracy; degeneracies between parameters are easily found, convergence criteria (already implemented in the code) ensure that statistical quantities for the parameters of interest are robustly determined and cross-checks through statistical analysis of mock catalogs are not necessary.
- its "user friendly" characteristics. The user does not need to decide *a priori* the number density of samples for each region, trying to find a compromise between the accuracy of the results and

the speed of the code: only the prior range must be chosen in advance for **CIGALEMC**; in fact the Metropolis-Hastings algorithm automatically samples adequately the posterior probability according to its values.

Our code will be available very soon at this web address: <http://www.oamp.fr/cigale/>.

7. ACKNOWLEDGEMENTS

P.S. would like to thank Denny Dale for very useful discussions. AA was supported by an appointment to the NASA Postdoctoral Program at the Ames Research Center, administered by Oak Ridge Associated Universities through a contract with NASA. We thank Antony Lewis for providing a publicly available version of **cosmomc**.

REFERENCES

- Acquaviva, V., Gawiser, E., Guaita, L., [arXiv:1101.3017](#)
 Balogh, M. L., Morris, S. L., Yee, H. K. C., et al. 1999, *ApJ*, 600, 681
 Buat, V. et al., (Herschel collaboration), *MNRAS Letters*, Volume 409, Issue 1, pp. L1-L6, (2010)
 Buat, V. et al., [arXiv:1102.157](#)
 Buat, V. et al., *in preparation*.
 Burgarella, D., Buat, V., & Iglesias-Páramo, J. 2005, *MNRAS*, 360, 1413
 Bruzual, G., & Charlot, S. 2003, *MNRAS*, 344, 1000
 Calzetti, D., Kinney, A.L., & Storchi-Bergmann, T. 1994, *ApJ*, 429, 582
 Cohen, J., *Statistical power analysis for the behavioral sciences* (1988)
 Calzetti, D., Armus, L., Bohlin, R.C., et al. 2000, *ApJ*, 533, 682
 Cannon, J. M. et al., *ApJ*, 647: 293-302, 2006
 Chary, R., & Elbaz, D. 2001, *ApJ*, 556, 562
 Christensen, N., Meyer, R., Knox, L., Luey, B., *Class. Quant. Grav.* 18, 2677 (2001)
 Conroy, C., Gunn, J. E., White, M., *ApJ*, 699: 486-506, 2009
 da Cunha, E., Charlot, S. & Elbaz, D., 2008, *MNRAS*, 388, 1595
 Dale, D.A., & Helou, G. 2002, *ApJ*, 576, 159
 Dale, D.A., Bendo, G.J., Engelbracht, C.W., et al. 2005, *ApJ*, 633, 857
 Dopita, M. A., Groves, B. A., Fischera, J., Sutherland, R. S. et al., 2005, *ApJ*, 619, 755
 Fioc, M., & Rocca-Volmerange, B. 1997, *A&A*, 326, 950
 Fitzpatrick, E.L., & Massa, D. 1990, *ApJS*, 72, 163.
 Fitzpatrick, E.L., & Massa, D. 2007, *ApJ*, 663, 320
 Gelman, A. & Rubin, D. B., *Statist. Sci.* Vol. 7, Number 4 (1992), 457-472
 Gil de Paz, A., Boissier, S., Madore, B. F., et al. 2007, *ApJS*, 173, 185
 Giovannoli, E., Buat, V., Noll, S., Burgarella, D., Magnelli, B., 2011 *A&A* 525, A150
 Jarrett, T.H., Chester, T., Cutri, R., Schneider, S.E., & Huchra, J.P. 2003, *AJ*, 125, 525
 Kennicutt, R. C. Jr., et al., 2003, *PASP*, 115, 928
 Kinney, A.L., Calzetti, D., Bohlin, R.C., et al. 1996, *ApJ*, 467, 38
 Kodama, T., & Arimoto, N. 1997, *A&A*, 320, 41
 Lagache, G., Dole, H., Puget, J.L., et al. 2003, *MNRAS*, 338, 555
 Lagache, G., Dole, H., Puget, J.L., et al. 2004, *ApJS*, 154, 112
 Lewis, A., & Bridle, S. 2002, *PRD* 66, 103511
 Li, A., & Draine, B. T. 2001, *ApJ*, 554, 778
 Li, A., & Draine, B. T. 2002, *ApJ*, 576, 762

- Maraston, C. 2005, MNRAS, 362, 799
Meiksin, A. 2006, MNRAS, 365, 807
Moustakas, J., & Kennicutt, R.C. Jr. 2006, ApJ, 651, 155
Muñoz-Mateos, J.C., Gil de Paz, A., Zamorano, J., et al. 2009, ApJ, 703, 1569
Noll, S., Mehlert, D., Appenzeller, I., et al. 2004, A&A, 418, 885
Noll S., Burgarella D., Giovannoli E., Buat V., Marcillac D., Munoz-Mateos J. C., 2009, A&A, 507, 1793
Raftery, A. E. & Lewis, S. M., Statistical Science, 7, 493-497.(1992)
Siebenmorgen & Krügel, 2007, A&A, 461, 445
Silva, L.; Granato, G. L., Bressan, A., Danese, L., 1998, ApJ, 509, 103
Stoughton, S., Lupton, R.H., Bernardi, M., et al. 2002, AJ, 123, 485
Witt, A.N., & Gordon, K.D. 2000, ApJ, 528, 799